A comparison of tectonics of the eastern Sierra Nevada, CA in the vicinity of Mt. Whitney and Lee Vining, using (U-Th)/He and $^4He/^3He$ thermochronometry: Preliminary results and thermal modeling

Trevor Hillebrand

Introduction

The eastern side of the Sierra Nevada displays striking variations in morphology. In the southeastern Sierra Nevada, Mt. Whitney and the surrounding peaks jut sharply out of the Owens Valley, exhibiting very steep stream channels that drain into the valley. North of Mt. Whitney, the range becomes more gently sloped, with long and wide river canyons grading into the valley over many miles. These different morphologies may be a result of different exhumation rates of the Sierran block along the eastern escarpment due to differences in rates or timing of tectonic uplift and erosional unroofing.

This paper describes ongoing isotope geochemical work using (U-Th)/He and $^4He/^3He$ thermochronometry that will serve to constrain the timing of the base-level drop of the Owens Valley relative to the Sierran block and the evolution of valleys in the eastern flank of the range. These data are taken from measurements on apatite crystals from Sierran granites and granodiorites collected along elevation transects of Whitney Portal Rd. and Tioga Pass from Lee Vining to Tioga Lake. The data provide cooling ages and time-temperature (t-T) histories of the rocks, which will help answer the question of the controlling factor in eastern Sierran geomorphology and provide constraints on the timing and progression of Basin and Range extension.

Literature Summary: The evolution of the Sierra Nevada

Emplacement and Characteristics of the Batholith

The Sierran Batholith consists of granitic plutons that were intruded into the crust between 270 and 80 Ma. The batholith has a relatively uniform thickness of 30-35 km, and an aspect ratio of at least five to one (Ague and Brimhall, 1988). The Mt. Whitney pluton was emplaced between 87 and 83 Ma, towards the end of regional magmatism (Maheo et al., 2004). The rocks of the northern field site at Lee Vining were mainly emplaced during the Scheelite Intrusion, 226-218 Ma, with some rocks emplaced during the Late Cretaceous by the Tuolumne Intrusion (Barth et al., 2011). Amphibole geobarometry by Ague and Brimhall (1988) shows a west-to-east decrease in crystallization pressure across the batholith, as well as a deep crustal emplacement of >23 km for the southern Sierra Nevada. The crust beneath the southern Sierra must be 60 to 90 km thick in order to prevent a surface expression of a thermal pulse from the cessation of subduction (Saltus and Lachenbruch, 1991). Ague and Brimhall (1988) demonstrate a strong crustal component to the granites of the eastern side of the batholith.

Fission track data were previously thought to show a low Cenozoic geothermal gradient of ~6 °C/km, but (U-T)/He data from House et al. (1997) shows that a moderate geotherm of ~25 °C/km is required for their age-elevation profile. Brady et al. (2006) attribute most or all of surface heat flow to radiogenic heat from within the batholith, as mantle heat flow has been very low since 5-10 m.y. after the cessation of subduction arc magmatism beneath the Sierra ~80 Ma (Dumitru et al., 1990). This cooling was likely caused by an eastward migration of magmatism due to a shallowing subduction angle, which caused the subducting plate to rise and cool the overriding crust.

Topographic Evolution

House et al. (1998) show that the Sierra Nevada had developed Andean-scale topography by 70-80 Ma. Uplift of the range may have begun as early around 185 Ma. They used (U-Th)/He ages from apatite to estimate the age of topographic relief, using the assumptions that river drainages impart a thermal structure in the crust beneath and that cooling thus occurs earlier beneath valleys than beneath ridges. The low closure temperature of the (U-Th)/He system in apatite makes this the best thermochronometer for the job. They found that cooling ages were most sensitive to long-wavelength (20-70 km) topography. The San Joaquin and Kings River drainages showed significant age variation from the surrounding high topography, but the smaller Tuolumne and Merced drainages had no effect on the helium ages, suggesting that either they were not formed by the time of cooling or they are too small to produce a change in the thermal structure of the crust beneath them.

House et al. (1998) found an average age variation of 20-30 Myr between ridges and valleys, suggesting long-wavelength relief of 2-4 km by 70-80 Ma. Because modern relief in the Sierra Nevada is ~1 km, with a mean elevation of 2.8 km, this suggests that (1) the average erosion rate of the ridges has been twice that of the valleys since 70 Ma, leading to a reduction in Cenozoic relief, and (2) mean elevation has decreased since 70 Ma.

Uplift of the Sierra was very rapid between 99 and 57 Ma (Wakabayashi and Sawyer, 2001). The range crest migrated eastward with the eastward progression of exhumation. Sediment accumulation rates in the Great Valley show that uplift and erosion rates were highest from 99-84 Ma, which coincides with the final stages of pluton emplacement. This was followed by a period of tectonic quiescence, perhaps due to eclogitic recrystallization of the mafic root of the batholith and an accompanying increase in density.

Laramide deformation and crustal thickening of the Great Basin, east of the Sierra Nevada, occurred between 80 and 45 Ma. Basin and Range extension may have begun on the eastern side of the northern Sierra ~35 Ma and progressed south. The Sierran microplate broke away from the western side of the Nevadaplano ~10-11 Ma (Busby and Putirka, 2009; Saleeby et al., 2009), as extensional faulting migrated westward to form the eastern escarpment that bounds the range today.

Westward tilting of the Sierran block may have initiated ~5 Ma (Wakabayashi and Sawyer, 2001), and the crest of the range migrated westward through the Pliocene (Bachman, 1978). Apatite (U-Th)/He ages show a possible period of very slow exhumation along the Sierra Nevada Frontal Fault until as late as 11 Ma, and ages from other normal faults nearby suggest a westward propagation of fault activity (Maheo et al., 2004). Basin and Range extension and the westward encroachment of the Walker Lane Belt may have acted to cause this western migration of the Sierran crest.

The uplift of the range along the eastern Sierra Frontal Fault is balanced on the western side of the microplate by subsidence and sedimentation in the western Great Valley, due to the rigid behavior of the microplate in the northern Sierra. However, this rigid behavior breaks down in the southernmost 100-150 km of the Sierra Nevada due to overriding of a lateral ramp in the subduction megathrust beneath. This break in the rigid behavior of the Sierran microplate results in a step-over in regional control of the westward tilt from the eastern escarpment system north of ~36.48°N to the Kern Canyon Fault system south of that latitude. The step-over is accompanied by internal deformation in the southernmost 100-150 km of the Sierran microplate (Saleeby et al., 2009).

The present topography of the Sierra Nevada is likely the result of a superposition of relict topography caused by tectonic and erosive processes during and since the late Cretaceous-early Cenozoic uplift and new topography from the ~ 5Ma uplift and tilting event (Wakabayashi and Sawyer, 2001; McPhillips and Brandon, 2012). High erosion rates accompanied the rapid pulse of uplift in the late Cretaceous. House et al. (1998) show that precursors to the modern canyons were formed at early as 70 Ma. During the period of tectonic quiescence ~57 – 15 Ma, erosion may have exceeded uplift, leading to a net decrease in elevation. From 80-45 Ma, the southern Sierra Nevada formed a barrier to west-flowing rivers, with elevations of greater than 2,500 m (Wakabayashi and Sawyer, 2001). This may show that the distinct difference in elevation and relief between the northern and southern Sierra Nevada developed during this time, before the Sierra broke off from the elevated Nevadaplano. Since westward tilting began ~5 Ma, the westward encroachment of the Walker Lane belt, stream incision, and extension in the Basin and Range have contributed to the significant relief of the eastern Sierra.

Strategy, Experimental Design, and Hypothesis

Samples were collected to be analyzed using (U-Th)/He and $^{4}He/^{3}He$ thermochronometry on apatite. The (U-Th)/He thermochronometer uses the concentrations of isotopes of these three elements to supply relative cooling ages of the rocks (Farley, 2002; House et al., 1997; House et al., 1998). An age-elevation profile created from these data facilitates approximation of exhumation rates. The $^{4}He/^{3}He$ thermochronometer involves stepwise degassing of apatite crystals that have been irradiated by an energetic proton beam to induce an even spatial distribution of ^{3}He (Shuster and Farley, 2005). The ratio of radiogenic ^{4}He to proton-induced ^{3}He provides additional constraints on the low-temperature cooling histories of these samples.

The degassing of ^{3}He serves to define the diffusion kinetics of helium within the crystal. The low closure temperature of the (U-Th)/He system in apatite makes these two thermochronometers sensitive to the low temperatures (from ~80°C down to 20°C) that are relevant to the cooling of Sierran plutonic rocks due to exhumation (Dodson, 1973; Shuster et al., 2011; House et al., 1997).

Samples of granitic rocks were collected from an elevation transect of the lower elevations of Mt. Whitney, Tioga Pass, and several points in between. Samples were selected for proximity to valleys, apparent lack of chemical weathering, and distance from late Cenozoic volcanics that could reset the helium age. In order to acquire enough apatite from mineral separation, samples had to be roughly football-sized or larger. Still, not all samples yielded sufficient amounts of apatite. Sampling locations are shown in Figure 1.

In order to analyze apatite for (U-Th)/He and $^{4}He/^{3}He$, I first had to separate the apatite from the rest of the sample. Each rock was crushed with a hammer, fed into a jaw crusher, and then run through a disc mill twice to achieve the desired size of < 0.5 mm. Each sample was then sieved in 70- and 230-mesh sieves to separate the size fraction appropriate for apatite. The largest and smallest size fractions were bagged and archived, and I continued working with the middle fraction. In order so separate out undesirable magnetic minerals, I put this middle fraction through the Frantz Isodynamic Separator at least twice, increasing from 0.5 to 2 A. The magnetic fraction was discarded, and the non-magnetic fraction was put in a heavy liquid of density 2.8 g/cm^{3} for 8-12 hours in order to separate the apatite from quartz, feldspars, and zircons, which are non-magnetic. The apatite, being denser than these other minerals, fell to the bottom of the column while the others floated. Some samples contained pyrite, in which case a

second density separation with a heavy liquid of 3.0 g/cm^3 was required. Some handpicking was also required in these cases.

To prepare single apatite crystals for ^{4}He/^{3}He analysis (Shuster and Farley, 2005), packets of ~100 mg of apatite from each sample were irradiated by an energetic proton beam in order to induce a spatially uniform concentration of ^{3}He within each grain. Single grains of each sample were then chosen for step-wise degassing. The criteria for selection were as follows: (1) euhedral crystal, (2) unfractured, (3) free of fluid inclusions, (4) radius of sphere with equivalent surface area-to-volume ratio > 55 microns (Shuster and Farley, 2005). Dimensions of selected crystals were measured to determine radius of the approximated sphere. The crystals were photographed under high magnification and placed in platinum packets, which were then placed in the sector field noble gas mass spectrometer and sequentially degassed with a feedback-control.

While helium ages from each sample are required in order to create a time-temperature path, we can use an estimated age for preliminary modeling. In this paper, I assume that the age-elevation relationship reported in House et al. (1997) is applicable to my Mt. Whitney field site, and use an age that they reported for a sample collected very close to one of my own samples. Using the HeFTy modeling software (Ketcham, 2005), I was able to perform forward and inverse modeling to achieve an estimated cooling path. The data used in the model is found in Table 1.

The inverse modeling used a Monte Carlo random search to generate possible cooling paths for the sample, using the assumed age and U and Th concentrations. The random search was allowed to run for 10^4 attempted paths, and displayed acceptable, good, and best-fit paths once finished. I applied constraints to the inversion, forcing the sample to cool below 200°C between 85 and 70 Ma. Rapid cooling due to primary magmatic cooling, underthrusting of the

cold Pacific Plate at the end of Sierran arc magmatism, and erosional unroofing requires this cooling constraint (House et al., 1997).

Though this modeling is preliminary due to the unavailability of the (U-Th)/He ages, there is good agreement between the model results and models and observations found in the previous literature. I hypothesize that with my own helium age and U and Th concentrations for this sample, the cooling path will not be considerably different from those used in this model. Cooling paths from the other samples along the Mt. Whitney transect will exhibit the same general features, but will be shifted along the temperature axis according to their elevation relative to this sample. The samples taken from Tioga Pass are from higher elevations, thus I expect to see that they cooled long before the Mt. Whitney samples. The onset of Basin and Range extension may also be captured in these data, which will give a rough estimate of the rate at which extensional faulting progressed south along the eastern Sierran escarpment.

Results so far

Figure 2 shows $^{4}He/^{3}He$ data from step-wise degassing of a sample collected from Whitney Portal Rd. at an elevation of 2274.4 m. The sample is assumed to have an uncorrected helium age in close agreement with House et al.'s (1997) sample that was collected <100 m vertical distance above. The uncorrected age of 25 Ma yields a corrected age of 32 ± 6.4 Ma, which is used in both the forward and inverse models. Age and goodness of fit (GOF) values for these models are summarized in Table 2.

Inverse modeling shows rapid cooling starting between 10 and 15 Ma, with greatest confidence in ages closer to 15 Ma (Figure 3). Out of 10,000 paths tried, the inverse model found 59 acceptable paths and 3 good paths. There are two criteria for a good path: (1) the mean

GOF must be greater than 0.5, and (2) GOF>1/(N+1), where N is number of GOF tests that were run. Acceptable paths have GOF > 0.05, and correspond to cooling histories that are not ruled out by the data (Ketcham, 2005). The best-fit time-temperature path given by the inverse model shows onset of rapid cooling at 15 Ma (Fig. 3), which is in agreement with House et al.'s (1997) age of 15 Ma for Basin and Range extension. The inverse model closely matches an age-paleodepth profile from Stockli et al. (2000), which shows the exhumation of a partial retention zone by extensional faulting of the White Mountains ~12 Ma. While the age-elevation profile calculated by House et al. (1997) records cooling until ~20 Ma, these new $^{4}He/^{3}He$ data record the rapid exhumation event at 15 Ma. Assuming the estimated helium age is very close to the actual helium age of this sample, this shows that extensional faulting of the eastern Sierran escarpment was roughly contemporaneous with extensional faulting across the Owens Valley.

Cooling is shown to have occurred at a constant rate since 15 Ma, so the tilting of the Sierran block at ~5 Ma described by Wakabayashi and Sawyer (2001) is not shown as a good path by the inverse model; however, forward modeling including this event is shown in Figure 5. It is assumed that westward tilting of the Sierran block would correspond to an increased rate of cooling at ~5 Ma. It is possible to achieve age and spectrum GOFs >0.05, so this is not ruled out by the data.

Cooling path envelopes for good and acceptable fits are shown in Figure 6. Many specific paths within these areas fail to fit the spectrum and age data, but this figure gives a schematic depiction of where the good and acceptable paths must fall. A slight difference in the actual helium age from my assumed age is more likely to change the specific paths than the shape of the overall path envelope, so this is useful for visualizing what this model will look like when all the data have been collected. The two paths shown over the envelopes in Fig. 5

represent end-member paths of acceptable fit that do not cross over to the other side of the good path envelope. The orange path shows slower cooling through the middle Cenozoic, with very rapid Basin and Range extension initiating at ~11 Ma, while the blue path shows rapid cooling to 82 Ma followed by a long, slow period of cooling through the partial retention zone, with Basin and Range extension initiating at 15 Ma.

Fig 1. Above: Google Earth image of locations of all thirteen samples. Southernmost cluster is from Mt. Whitney. Northernmost cluster is from Tioga Pass Rd.

Below: Sample location for THES-13, which is the sample discussed in this paper. The sample was taken from a road cut on Whitney Portal road. Largest mountain symbol is at the peak of Mt.Whitney. Sample elevation is 2274.4 m.


THES-13
Lone Pine
S Main St
© 2012 Google
Image USDA Farm Service Agency
Image © 2012 DigitalGlobe
Image © 2012 GeoEye
Google

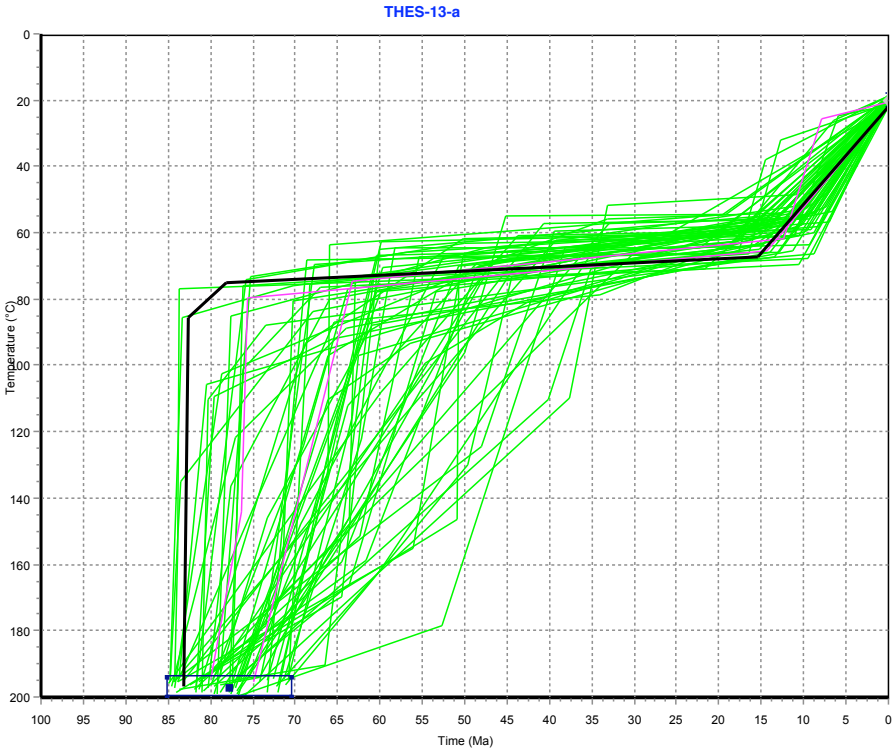

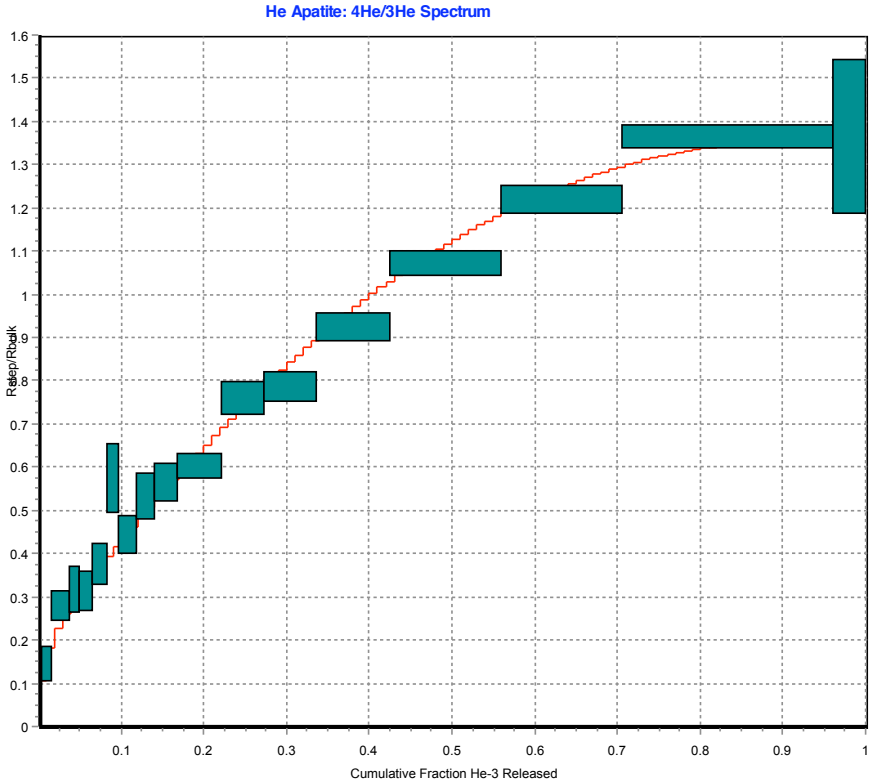

Fig 2. Above: Inverse modeling of possible time-temperature paths for a sample collected from Mt. Whitney, CA. Helium age is assumed to be 32 ± 6.4 Ma, after House et al. (1997). Good paths are in pink, acceptable paths are green, and the solid black line is the best-fit path.

Below: $^{4}He/^{3}He$ spectrum data from step-wise degassing of an apatite crystal. Cumulative ^{3}He release fraction is on the horizontal axis. The vertical axis is the $^{4}He/^{3}He$ of each step normalized to the bulk $^{4}He/^{3}He$ of the sample. The red line shows the goodness of fit of the best-fit path determined by inverse modeling.

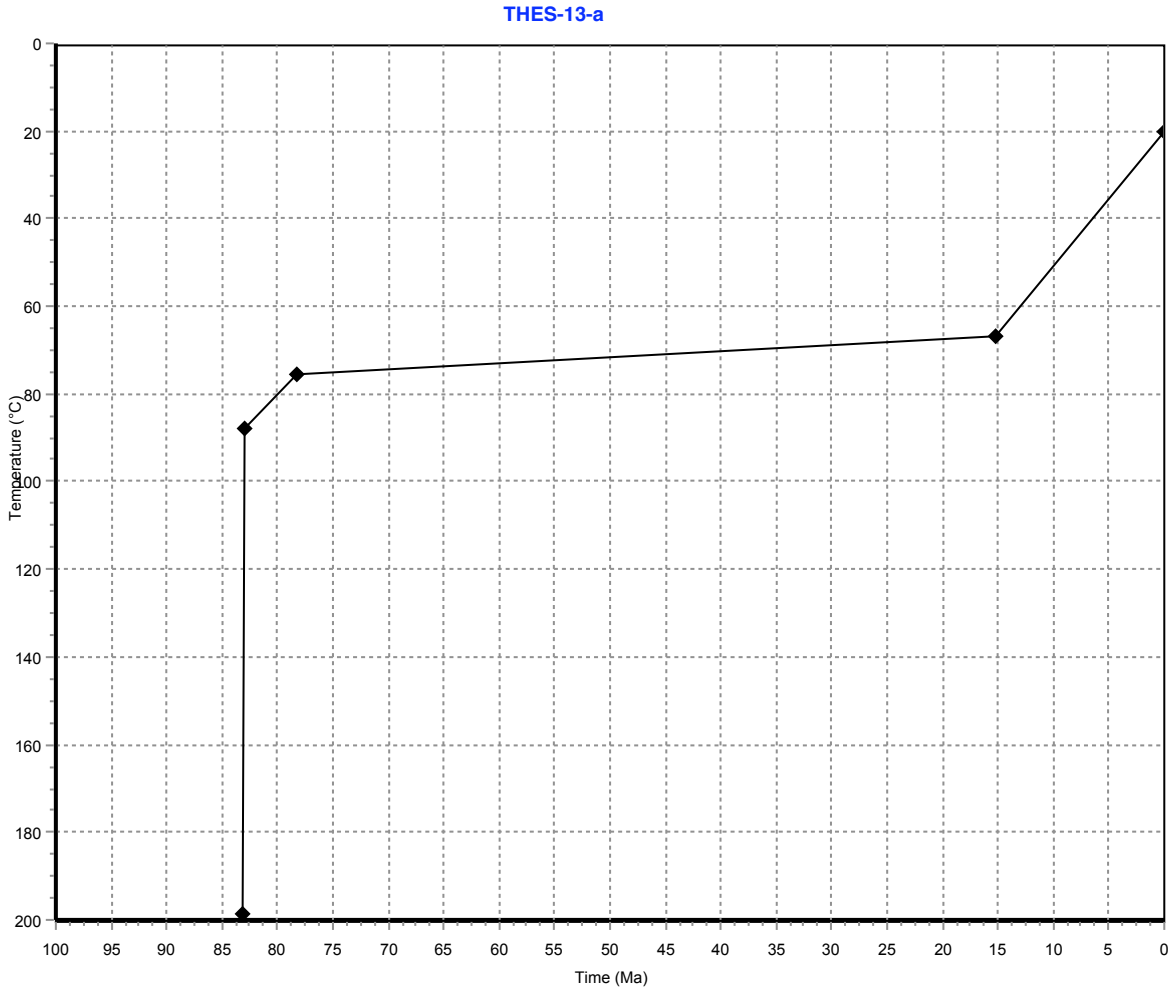

Fig 3. Best-fit cooling path from inverse modeling. Onset of Basin and Range extension is shown as break in slope at 15 Ma. Rapid cooling from 83-78 Ma is the product of primary magmatic cooling, underthrusting of the cold Pacific Plate, and erosional unroofing. This model gives a helium age of 31.6 Ma. Age GOF = 0.95. Spectrum GOF = 0.53.

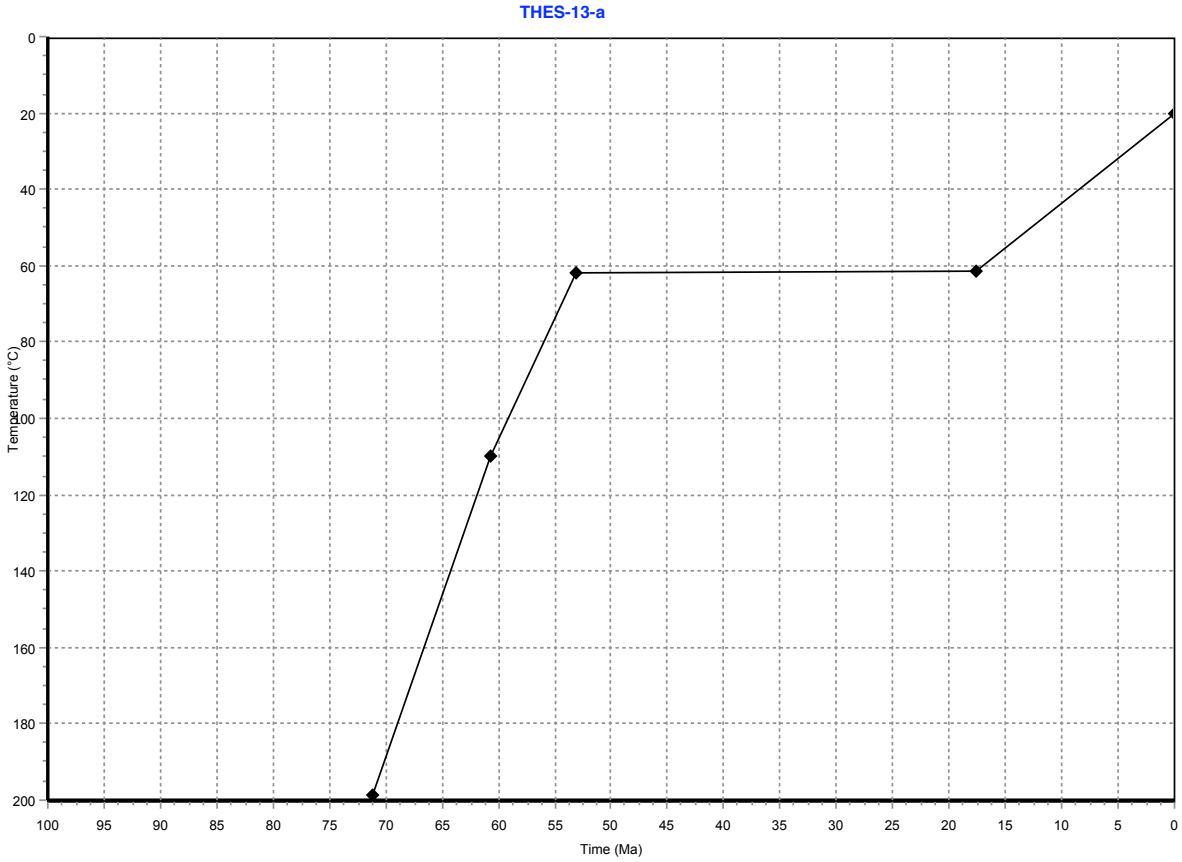

Fig. 4: An alternate good path chosen by inverse modeling. Cooling is rapid—but much slower than the best-fit path—through the early Cenozoic, with no cooling from 53 to 17 Ma. Onset of Basin and Range extension occurs at 17 Ma and rapid cooling resumes. Calculated model helium age is 32 Ma; GOF = 1.00. Spectrum GOF = 0.44.

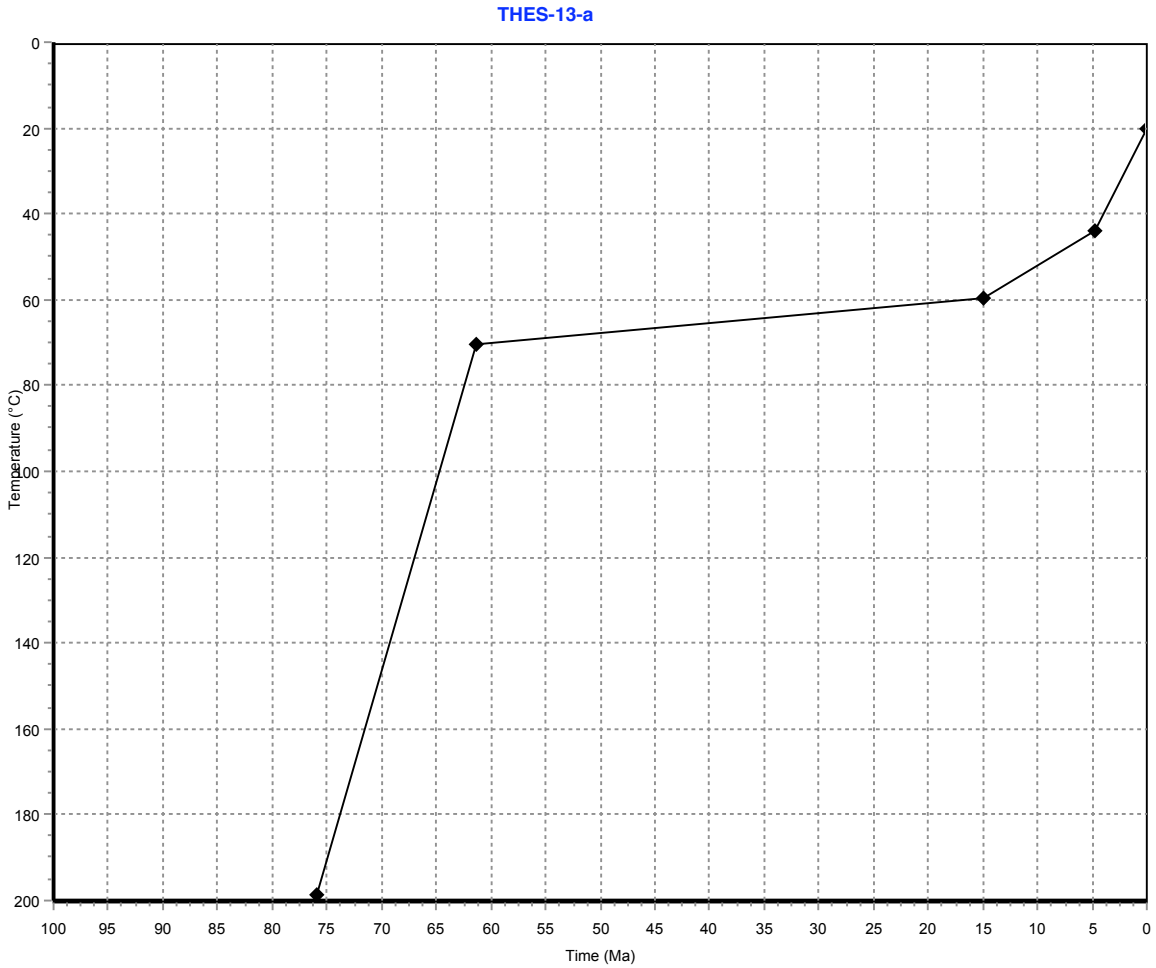

Fig 5. A cooling path incorporating increased cooling rate at ~5 Ma due to westward tilting of the Sierran block, from Wakabayashi and Sawyer (2001). The model is not able to achieve a spectrum GOF above 0.25, but the path is not ruled out by the data. The path shown above has an age of 32.2, with age GOF = 0.97 and spectrum GOF = 0.12.

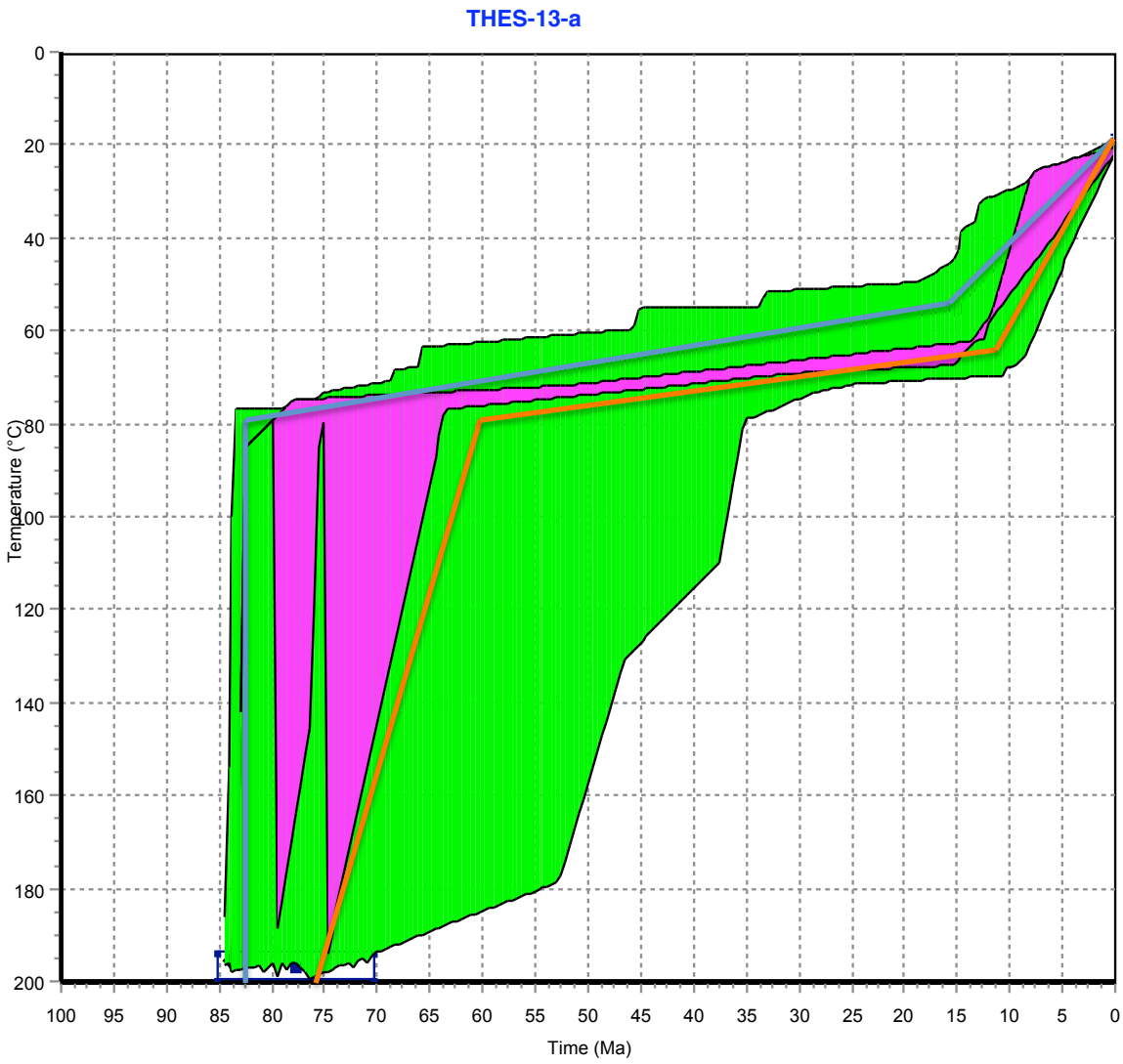

Fig 6: Cooling path envelopes showing areas of good (pink) and acceptable (green) fit to the age and $^{4}He/^{3}He$ spectrum data. A path along the top (low T) of the acceptable area is shown in blue and gives an age of 42.6, with an age GOF of 0.1 and a spectrum GOF of 0.06. GOF is most sensitive to movement of the break in slope at 15 Ma. When moved to 10 Ma at temperatures within the partial retention zone, one or both GOF values fall close to zero. A path along the lower side (high T) of the green envelope (shown in orange) gives an age GOF of 0.07 and a spectrum GOF of 0.59.

Table 1: $^{4}He/^{3}He$ data from stepwise degassing of an apatite crystal from Mt. Whitney. Age and bulk U and Th concentrations are taken from House et al., 1997.

Sample name	Grain radius (cm)	bulk [U] (ppm)	bulk [Th] (ppm)	age	delage	
THES-13-a	0.00664	50	50	25	5	
Latitude: 36.596010°	Longitude: -118.21277°	Elevation: 2274.4 m				
Step	T (deg C)	t (hr)	He-3 (10^6 atoms)	dHe-3 (10^6 atoms)	4/3_ratio	d4/3_ratio
1	210	0.2	0.002	0	1601.64	66080
2	225	0.5	0.046	0.004	204.42	296
3	260	0.38	0.133	0.01	417.85	112
4	300	0.51	0.222	0.014	789.78	94
5	300	0.66	0.145	0.01	900.06	146
6	310	0.66	0.174	0.012	885.65	124
7	330	0.46	0.188	0.012	1060.79	130
8	340	0.45	0.149	0.01	1615.76	219
9	350	0.48	0.241	0.015	1250.01	121
10	350	0.66	0.23	0.014	1499.33	144
11	370	0.53	0.297	0.017	1593.31	122
12	400	0.48	0.588	0.025	1695.31	81
13	410	0.5	0.562	0.024	2134.7	102
14	420	0.56	0.68	0.027	2212.15	95
15	440	0.63	0.983	0.033	2593.7	88
16	475	0.5	1.465	0.041	3007.75	81
17	500	0.5	1.603	0.043	3414.9	87
18	600	0.5	2.773	0.057	3823.84	72
19	700	0.5	0.423	0.021	3823.84	500
20	800	0.5	0.01	0.001	3823.84	500

Table 2: Summary of model ages and GOF values.

	Best-fit	Alternate Good fit	Acceptable: Blue	Acceptable: Orange	5 Ma tilt
Age of model	31.9	32	42.6	20.2	32.2
Measured Age	32.0 ± 6.4	32.0 ± 6.4	32.0 ± 6.4	32.0 ± 6.4	32.0 ± 6.4
Age GOF	0.99	1.00	0.1	0.07	0.97
Spectrum GOF	0.54	0.44	0.06	0.59	0.12

References

1. Ague, J., and Brimhall, G. H, 1988, Regional variations in bulk chemistry, mineralogy, and the compositions of mafic and accessory minerals in the batholiths of California, Geol. Soc. Amer. Bull., v. 100, 891-911

2. Ague, J. and Brimhall, G. H, 1988, Magmatic arc asymmetry and distribution of anomalous plutonic belts in the batholiths of California: Effects of assimilation, crustal thickness, and depth of crystallization, v. 100, 912-927.

3. Bachman, S. B. Pliocene-Pleistocene Break-up of the Sierra Nevada–White-Inyo Mountains Block and Formation of Owens Valley. *Geology* 6.8 (1978): 461-463.

4. Barth, A. P., Walker, J. D., Wooden, J. L., Riggs, N. R., Schweickert, R. A. Birth of the Sierra Nevada magmatic arc: Early Mesozoic plutonism and volcanism in the east-central Sierra Nevada of California. *Geosphere* vol. 7 no. 4 (2011): 877-897.

5. Brady, R., M. Ducea, S. Kidder, and J. Saleeby. The Distribution of Radiogenic Heat Production as a Function of Depth in the Sierra Nevada Batholith, California. *Lithos* 86.3-4 (2006): 229-44

6. Busby, C.J. and Putirka, K. Miocene evolution of the western edge of the Nevadaplano in the central and northern Sierra Nevada: palaeocanyons, magmatism, and structure. *Internat. Geology Review*. Vol. 51, Nos. 7 – 8. 670-701. 2009.

7. Dodson, M.H. Closure Temperature in Cooling Geochronological and Petrological Systems. *Contr. Mineral. And Petrol.* Vol 40 (1973), 259-274.

8. Dumitru, T.A. Subnormal Cenozoic Geothermal Gradients in the Extinct Sierra Nevada Magmatic Arc: Consequences of Laramide and Post-Laramide Shallow-Angle Subduction. *Journal of Geophysical Research* 95.B4 (1990): 4925-4941.

9. Farley, K.A. (U-Th)/He Dating: Techniques, Calibrations, and Applications. *Reviews in Mineralogy and Geochemistry* vol 47 no. 1 (2002). 819-844

10. House, M. A., B. P. Wernicke, and K. A. Farley. Dating Topography of the Sierra Nevada, California, Using Apatite (U-Th)/He Ages. *Nature* 396 (1998): 66-69.

11. House, M. A., B. P. Wernicke, K. A. Farley, and T. A. Dumitru. Cenozoic Thermal Evolution of the Central Sierra Nevada, California, from (U-Th)/He Thermochronometry. *Earth and Planetary Science Letters* 151 (1997): 167-179.

12. Ketcham, R.A. Forward and Inverse Modeling of Low-Temperature Thermochronometry Data. *Reviews in Mineralogy & Geochemistry.* Vol. 58 (2005). pp. 275-314

13. Maheo, G., K. A. Farley, and M. A. Clark. Cooling and Exhumation of the Sierra Nevada Batholith in the Mount Whitney Area (California) Based on (U-Th)/He Thermochronometry. *Eos Trans. AGU Fall Meeting* 85.47 (2004).

14. McPhillips, D. and M.T. Brandon. Topographic evolution of the Sierra Nevada measured directly by inversion of low-temperature thermochronometry. *American Journal of Science.* Vol 312 (2012), p. 90-116.

15. Saleeby, J., Z. Saleeby, E. Nadin, and G. Maheo. Step-over in the Structure Controlling the Regional West Tilt of the Sierra Nevada Microplate: Eastern Escarpment System to Kern Canyon System. *International Geology Review* 51.7 (2009): 634-669.

16. Saltus, R. W., and A. H. Lachenbruch. Thermal Evolution of the Sierra Nevada: Tectonic Implications of New Heat Flow Data. *Tectonics* 10.2 (1991): 325-344.

17. Shuster, D. L., and K. A. Farley. 4He/3He Thermochronometry: Theory, Practice, and Potential Complications. *Reviews in Mineralogy and Geochemistry* 58.1 (2005): 181-203.

18. Shuster DL, Cuffey KM, Sanders JW, Balco G. Thermochronometry reveals headward propagation of erosion in an alpine landscape. *Science* Vol. 332 no. 6025 pp. 84-88 (2011)

19. Stockli, D. F., K. A. Farley, and T. A. Dumitru. Calibration of the Apatite (U-Th)/He Thermochronometer on an Exhumed Fault Block, White Mountains, California. *Geology* 28.11 (2000): 983-86.

20. Wakabayashi, J., and Sawyer, T.L., 2001, Stream incision, tectonics, uplift, and evolution of topography of the Sierra Nevada, California: Journal of Geology, v. 109, p. 539-562.